Heightened dynamics of the oxidized Y48H variant of human cytochrome *c* increases its peroxidatic activity

Oliver M. Deacon[1], Andreas Ioannis Karsisiotis[1], Tadeo Moreno-Chicano[1], Michael A. Hough[1], Colin Macdonald[2], Tharin M.A. Blumenschein[2], Michael T. Wilson[1], Geoffrey R. Moore[2*], Jonathan A.R. Worrall[1*]

[1]School of Biological Sciences, University of Essex, Wivenhoe Park, Colchester, CO4 3SQ, U.K. [2]School of Chemistry, University of East Anglia, Norwich Research Park, NR4 7TJ, U.K.

***To whom correspondence should be addressed:**

Geoffrey R. Moore: g.moore@uea.ac.uk; Tel: +44 1603 592003

Jonathan A.R. Worrall: jworrall@essex.ac.uk; Tel: +44 1206 872095

ABSTRACT

Proteins performing multiple biochemical functions are called 'moonlighting proteins' or extreme multifunctional (EMF) proteins. Mitochondrial cytochrome *c* is an EMF protein that binds multiple partner proteins to act as a signalling molecule, transfers electrons in the respiratory chain, and acts as a peroxidase in apoptosis. Mutations in the cytochrome *c* gene lead to the disease thrombocytopenia, which is accompanied by enhanced apoptotic activity. The Y48H variant arises from one such mutation and is found in the 40-57 Ω-loop, the lowest unfolding free energy sub-structure of the cytochrome *c* fold. A 1.36 Å resolution X-ray structure of the Y48H variant reveals minimal structural changes compared to the wild type structure, with the axial Met80 ligand coordinated to the heme iron. Despite this, the intrinsic peroxidase activity is enhanced implying that a pentacoordinate heme state is more prevalent in the Y48H variant, corroborated through determination of a Met80 'off-rate' of > 125 s^{-1} compared to ~ 6 s^{-1} for the wild type protein. Heteronuclear NMR measurements with the oxidised Y48H variant reveal heightened dynamics in the 40-57 Ω-loop and the Met80 containing 71-85 Ω-loop relative to the wild type protein, illustrating communication between these sub-structures. Placed into context with the G41S cytochrome *c* variant, also implicated in thrombocytopenia, a dynamic picture associated with this disease relative to cytochrome *c* is emerging whereby increasing dynamics in sub-structures of the cytochrome *c* fold serve to facilitate an increased population of the peroxidatic pentacoordinate heme state of the order, wild type < G41S < Y48H.

INTRODUCTION

The discovery that many proteins have more than one biological function was an important advance in understanding how complex organisms can have relatively few genes to carry out the many thousands of biochemical functions that occur within it [3, 4]. Jeffery listed a variety of mechanisms by which the function of a protein can switch between its different activities – and termed this ability 'moonlighting' [6]. In addition to genetic origins governing expression, these mechanisms included: differential localization within the cell, intracellular versus extracellular location, oligomerization, variable ligand/substrate concentrations, chemical regulation of activity, different binding sites for different partner molecules, and being part of different multi-protein complexes [6]. Advances in the field have led to the recent suggestion that the phrase 'extreme multifunctional proteins' (EMF) be employed instead of moonlighting proteins [7]. The rebranding is to create focus on the functional aspects of the phenomenon, rather than the mechanistic, noting that what makes moonlighting proteins worth studying is that they perform diverse functions and so that is what their definition should emphasize [8]. However, from a chemical perspective it is important to understand how moonlighting or EMF proteins operate. Energy landscape theory [9] suggests that one way a protein could moonlight is if the ground-state structure, which is the prevalent form under physiological conditions, is in equilibrium with one or more higher-energy forms of different structure present in small amounts. Such excited states of proteins have been identified in numerous systems in recent years, particularly through studies of protein folding, but also in ligand binding and enzyme catalysis [10, 11], and thus it is reasonable to think that this offers a route to enable proteins to moonlight.

Cytochrome *c* (Cc) is well known for its role in mitochondrial electron-transfer as an electron carrier between the cytochromes bc_1 and aa_3 complexes [12] but it also plays two important roles in apoptosis [13, 14]. One role is as a peroxidase to oxidise lipids as part of the process of creating a pore in the outer mitochondrial membrane [15], and the second set of roles is as a component of various multiprotein complexes, including: the cytoplasmic apoptosome multi-protein complex [16], heat shock protein 27 [17] and inositol triphosphate receptors in the endoplasmic reticulum [18]. Cc also functions as an inhibitor of a histone chaperone activity in the nucleus following DNA damage by binding to a nucleosome assembly protein [19] and as an extracellular ligand to serum leucine-rich alpha-2-glycoprotein-1 [20], an interaction that helps lymphocytes to survive from the toxicity resulting from Cc being released from cells undergoing apoptosis. From the structural information available, it appears that Cc in its role as a histone chaperone inhibitor [19] and as a component of the apoptosome [21] binds to the

relevant partner proteins at sites overlapping its binding sites for the cytochromes bc_1 and aa_3 complexes [22, 23]. Thus, in these moonlighting roles Cc appears to fit in well with the possible mechanisms given by Jeffery [6]. However, to turn Cc from an electron carrier into a peroxidase requires a major change in the way the heme group interacts with the polypeptide chain. The electron-transfer form of Cc, which we can call the ground state conformation, possesses a hexacoordinate heme iron with the side chains of His18 and Met80 acting as the axial heme iron ligands. To act as a peroxidase, Cc needs a pentacoordinate heme to allow the Fe(III) to react directly with H_2O_2, and it is this pentacoordinate state that we have suggested is the poorly populated excited state in equilibrium with the ground state [1].

Mutations in the human Cc (hCc) gene (*CYCS*) give rise to an inherited autosomal dominant disease, thrombocytopenia 4 (THC4; OMIM 612004), which is accompanied by enhanced mitochondrial apoptotic activity [24]. To date three mutations have been identified in the *CYCS* gene that give rise to the G41S, Y48H and A51V protein variants [24-26]. We, and others, have shown that the oxidized form of the hCc G41S variant has a greater intrinsic peroxidase activity than the wild-type (WT) protein [27, 28]. Furthermore, using NMR and azide binding kinetics we have shown that an equilibrium exists between the hexacoordinate ground state and a pentacoordinate excited state, with more of the G41S variant in the excited state than for the WT protein [1]. Here we report on studies of the second pro-apoptotic variant of hCc, Y48H, and show for the ferric form even more of this variant is in the excited pentacoordinate state than the G41S variant, and that this population difference is correlated with their relative stabilities and peroxidase activities.

MATERIALS AND METHODS

Site-directed mutagenesis and purification of the Y48H human cyt c variant

The Y48H variant of hCc was constructed using the Quikchange mutagenesis (Stratagene) protocol. The forward and reverse mutagenic primers were as follows: 5'-GCC CCT GGA TAC TCT CAT ACA GCC GCC AAT AAG AAC-3' and 5'-GTT CTT ATT GGC GGC TGT ATG AGA GTA TCC AGG GGC-3', respectively. A PCR mix consisting of primers (75 ng/µl), the wild-type template (15 ng/µl), 10 mM dNTPs (Fermentas), PFU Turbo polymerase (Stratagene), 10 X Pfu Buffer (Agilent) and deionisied water to give a final volume of 50 µl was prepared and subjected to the following PCR cycle; 95 °C – 3 min, (95 °C – 1 min, 65 °C – 1 min, 72 °C – 6 min) x18, 72 °C – 10 min. Over-expression of the Y48H variant together with the wild-type and G41S variant in *Escherichia coli* were carried

out in BL21(DE3) RIL (Invitrogen) cells with isolation and purification carried out as reported previously [27].

Protein preparation

Oxidized Cc proteins were prepared by the addition of excess $K_3[Fe(CN)_6]$, followed by removal of $K_3[Fe(CN)_6]$ and $K_4[Fe(CN)_6]$ and exchange into a desired buffer using a PD-10 column (GE Healthcare). Protein concentration was determined with a Cary 60 spectrophotometer (Agilent) and a molar extinction coefficient of ε = 106 mM^{-1} cm^{-1} at 409 nm.

Chemical denaturation and alkaline pH titrations

Far-UV CD spectra at 15 ^{o}C for oxidized Cc proteins (20 μM) in 10 mM potassium phosphate, 50 mM potassium fluoride pH 6.5 were recorded in the wavelength range 250-190 nm with an Applied Photophysics Chirascan CD spectrophotometer (Leatherhead, UK). Oxidized Cc stabilities were determined by titrating a 6 M stock solution of guanidine hydrochloride (GuHCl) (Fluka) to a 20 μM protein sample and the changes in molar ellipticity at 222 nm (θ_{222nm}) monitored. All titrations were carried out in triplicate. The fraction unfolded (F_u) at any given [GuHCl] was determined [29] and the free energy of unfolding (ΔG_{unf}) and dependence of ΔG_{unf} on denaturant concentration (*m* value) calculated using an equation for a two-state unfolding process [2]. The pH dependence of the 695 nm band in the UV-visible spectrum was monitored at room temperature by determining its absorbance at various values of pH for a solution of 100 μM oxidized Cc in a quartz cuvette (Hellma) with a small aliquot of $K_3[Fe(CN)_6]$ present to maintain an oxidising environment. The pH of the buffer (20 mM sodium phosphate pH 6.0) was adjusted with microliter aliquots of 1 M NaOH and measured after each addition using a semi-micro glass pH electrode. pH titrations were repeated up to three times and with different batches of proteins. Data were fitted to a one-proton ionization equilibrium equation to yield an apparent pK_a.

Preparation of liposomes and peroxidase assays

The phospholipids 1,1',2,2'-tetraoleoyl cardiolipin (TOCL) and 1,2-dioleoyl-*sn*-glycero-3-phosphocholine (DOPC) (AVANTI Polar Lipids, USA) were mixed in a 1:1 ratio and vortexed with the appropriate amount of buffer (20 mM sodium phosphate pH 6.5) and sonicated for 5 min in a high power sonicating water bath filled with ice-cold water to give

the desired stock concentration as previously described [27]. Peroxidase assays of the ferriCc proteins were carried out in the absence and presence of liposomes using H_2O_2 (Sigma) and 2,2-Azinobis(3-ethylbenthiazoline-6-sulfonic acid) (ABTS) (Sigma). The oxidation of ABTS was monitored at 730 nm on a Hewlett-Packard 8453 diode-array spectrophotometer scanning between 190 and 1100 nm and thermostatted at 20 ^{o}C. The reaction was initiated by the addition of 1 mM H_2O_2 (after 40 s) to a series of cuvettes containing 5 μM ferriCc and 200 μM ABTS with or without 25 μM TOCL/DOPC from a 2.5 mM stock. Using the wavelength pair 475-730 nm the slope of each trace (post-lag phase) was determined to obtain a rate in AU/s. The rate of ferriCc turnover is reported in s^{-1} obtained by dividing AU/s by the product of the concertation of oxidized ABTS (ε = 14 mM^{-1} cm^{-1}) and the total protein concentration of 5 μM. All assays were carried out in triplicate with errors reported as the standard error.

Stopped-flow kinetics

An Applied Photophysics (Leatherhead, UK) SX20 stopped-flow spectrophotometer thermostatted at 25 ^{o}C and equipped with both photomultiplier and diode array detection systems was used to monitor the kinetics of azide (N_3^-) binding to the oxidized Y48H hCc variant. A stock solution of 2 M sodium azide (Sigma) were prepared in 50 mM MES pH 7.0 and diluted to the desired [N_3^-] with the same buffer containing 2 M NaCl to maintain the ionic strength. Reaction time-courses were taken at 420 nm with [N_3^-] varying between 0.08 and 2 M before mixing and 10 μM protein (before mixing). All transients were fitted to a single exponential function yielding both pseudo first-order rate constants and amplitudes.

Crystallisation and X-ray structure determination

Crystals were grown using the sitting-drop vapour diffusion method at 18 ^{o}C. A 0.2 μl solution containing 56 mg/ml of oxidized Y48H Cc variant in 20 mM sodium phosphate pH 6.5 was mixed with an equal volume of reservoir solution (33 % PEG6000, 100 mM Tris/HCl pH 7.5) using a Crystal Gryphon robot (Art Robbins Instruments). Crystals were transferred to a cryoprotectant solution containing the reservoir solution and 15 % glycerol, before flash cooling by plunging into liquid nitrogen. Crystallographic data were measured at the Swiss Light Source (SLS, Villigen, Switzerland) at beamline X10SA using a Pilatus 6M-F detector (Dectris) and an X-ray wavelength of 1.0 Å. Data were indexed using XDS [30] and scaled and merged using Aimless [31] in the CCP4 suite with the CCP4i2 interface. The structure was

solved by molecular replacement in Phaser [32] using the WT hCc structure [27] (pdb code 3zcf) as the search model. The structure was refined with Refmac5 [33], with model building between refinement cycles in Coot [34]. Riding hydrogen atoms were added when refinement of the protein atoms had converged. Structures were validated using the Molprobity server [35] the JCSG Quality Control Server and tools within Coot [34]. Structural superpositions were carried out using GESAMT in CCP4i2 [36]. Coordinates and structure factors were deposited in the RCSB Protein Data Bank with entry 5O10. A summary of data, refinement statistics and the quality indicators for the structure is given in Table 1.

Table 1: Crystallographic data processing and refinement statistics for the Y48H hCc variant. Values in parenthesis refer to the outermost resolution shell 1.39-1.36 Å.

Parameter	hCc Y48H
Space group	$P2_1$
Unit cell	a = 56.9, b = 36.5, c = 60.7 Å, β = 116.7°
Resolution (Å)	1.36
R_{merge}	0.072 (1.115)
Unique reflections	45812 (2124)
Mn (I/SD)	13.3 (1.4)
$CC_{1/2}$	0.998 (0.512)
Completeness (%)	95.3 (90.2)
Redundancy	6.2 (5.4)
R_{cryst}	0.144
R_{free}	0.175
RMS dev. bond lengths (Å)	0.015
RMS dev. bond angles (°)	2.18
Ramachandran favoured (%)	97.0
Accumulated dose (MGy)	2.54
PDB accession code	5O10

NMR spectroscopy

All NMR data were collected with a Bruker 500 MHz (H/D exchange) or 800 MHz (1D, ^{15}N-relaxation and sequence specific assignments) spectrometer, both equipped with 5 mm HCN inverse triple resonance z-axis gradient probes. Samples for 1D ^{1}H NMR spectroscopy were oxidized and buffer exchanged into 20 mM sodium phosphate pH 6.5 and freeze dried.

Samples were redissolved in 500 µl of 99.9 % D_2O (sigma) and allowed to deuterate at room temperature for ~ 72 h. 4,4-dimethyl-4-silapentane-1-sulfonic acid (DSS; Sigma) (200 µM final concentration) and $K_3[Fe(CN)_6]$ (100 µM final concentration to maintain an oxidising environment) were added to each sample and 1D spectra were recorded at temperatures ranging from 288 to 313 K using presaturation to supress the solvent signal and with spectral widths of 20 and 80 ppm. Spectra were processed in Topsin (Bruker Biospin).

Single (^{15}N) and doubly (^{13}C,^{15}N) labelled samples of the Y48H hCc variant were prepared using procedures previously described [37]. NMR samples of the oxidized Y48H variant were prepared in 20 mM sodium phosphate pH 6.5 and contained 1 mM protein with 10 % D_2O (Sigma) for the lock. A set of 2D [^1H, ^{15}N]-HSQC and 3D HNCACB and CBCA(CO)NH spectra were recorded at 288 K and processed in Topsin (Bruker Biospin). Sequence specific assignments were obtained using the CCPNmr Analysis [38] and Sparky [39] programs.

H/D exchange NMR data was acquired at 288 K. Freeze-dried samples of the oxidized Y48H variant (1 mM) were re-dissolved in 20 mM sodium phosphate pH 6.5, 50 mM NaCl pre-made in 99.9 % D_2O (Sigma). Spectra were recorded as matrices of 1024 x 64 complex data points with 4 scans and spectral widths of 15 (^1H) and 42 (^{15}N) ppm centred at 4.7 and 118.6 ppm, respectively. The acquisition of consecutive [^1H, ^{15}N]-HSQC spectra started ~ 5 min after sample resuspension. Acquisition proceeded with consecutive HSQC spectra of ~ 5 min acquisition time for a period of 134 h, totalling 191 experiments. The first 100 experiments were collected with a 10 s delay between each to ensure maximum coverage of the fast-exchanging residues, with the following 74 experiments at 45 min intervals, followed by 17 experiments at 4 h intervals. CCPNmr Analysis [38] was used to fit peak volumes as a function of time to a single exponential decay function to yield decay rates from which protection factors (PFs) were calculated [40, 41] (Table S1). The free energies of exchange (ΔG_{ex}) were calculated from $\Delta G_{ex} = -RT\ln(PF)$ where R is the gas constant and T is the temperature in Kelvin [41] (Table S1).

^{15}N T_1, T_2 and [^1H]-^{15}N NOE data were collected at 288 K with spectra acquired as matrices of 1024 x 256 complex data points and 8 scans for T_1 and T_2 data and 64 scans for [^1H]-^{15}N NOE data. Spectral widths of 15 (^1H) and 39.3 (^{15}N) ppm centred at 4.7 and 118.6 ppm, respectively, were used. T_1 experiments were acquired with relaxation delays of 20, 50, 80, 200, 500, 750, 2000 and 3500 ms with duplicates at 20, 200 and 500 ms. T_2 experiments were acquired with relaxation delays of 16.96, 33.92, 50.88, 67.84, 101.76, 135.68, 203.52

and 254.40 ms with duplicates at 16.96, 50.88 and 101.76 ms. Recycle delays for both experiments were 5 s. The repeated relaxation delays were used for the determination of peak height uncertainties [42]. Both the T_1 and T_2 series of experiments were acquired as a pseudo-3D experiment and processed as individual planes 2D planes using NMRPipe [43]. Residues with peak overlap or weak intensity were excluded from the analysis. T_1 and T_2 values were extracted through the fitting of peak heights as a function of time to a single exponential function in CCPNmr Analysis [38]. These were subsequently converted to R_1 and R_2 rate constants ($R_1 = 1/T_1$ and $R_2 = 1/T_2$). The fit errors for T_1 and T_2 were also converted into R_1 and R_2 errors through the equality of the T_1/T_2 and R_2/R_1 errors. Heteronuclear [^{1}H]-^{15}N NOEs were measured with a proton saturation period of 5 s. Interleaved saturated and unsaturated experiments were acquired in triplicate to determine the experimental errors as the standard deviation of the average NOE value. NOE values were calculated as the ratio of peak heights with and without proton saturation.

RESULTS

*X-ray structure of the pro-apoptotic Y48H hCc variant*The X-ray structure of the Y48H variant of hCc was determined to 1.36 Å resolution. A space group of $P2_1$ was determined with two hCc molecules found in the crystallographic asymmetric unit, contrasting with the reported X-ray structures of the WT protein [27] and G41S variant [44], both of which had a P_1 space group and four hCc molecules in the asymmetric unit. The diffraction-weighted dose [45] incurred during collection of the high-resolution X-ray dataset for the Y48H variant was 2.54 MGy, a dose greatly exceeding that required to fully reduce ferric heme proteins to the ferrous form (typically 10s-100s kGy) [46, 47]. Hence, while the crystals were obtained from solutions of the ferric protein, in light of the extensive previous studies, measuring the doses typically required for ferric to ferrous heme protein reduction, we consider the structure to likely be predominantly that of the ferrous state. It is important to note that earlier X-ray studies of tuna Cc [48] and *Saccharomyces cerevisiae* iso-1 Cc [49] with much lower X-ray doses than the present study show that the conformation of the protein is largely independent of the heme oxidation state. Electron density in the heme region is consistent with a hexacoordinate species, with the Nε2 atom of His18 and the Sδ atom of Met80 coordinating the heme iron. The overall fold of each molecule in the asymmetric unit is identical to that of the WT protein and the G41S variant, with an overall RMS deviation in Cα positions of 0.18 Å between the three X-ray structures (Figure 1A). It is noted that the Cα deviation between residues 37-61

increases to 0.27 Å. Replacing Tyr48 with a His residue alters a H-bonding arrangement involving the heme propionates. In the WT protein structure the OH group of the Tyr48 side chain forms a H-bond (2.57 Å) to the O1A atom of heme propionate-7 [27]. Such an interaction is lost in the Y48H variant and the Nδ1 atom of the His48 side chain is favourably orientated to form a medium length polar interaction with the O2D atom of the heme propionate-6 (3.19 Å) (Figure 1B). The number of H-bond interactions with the OD2 atom of heme propionate-6

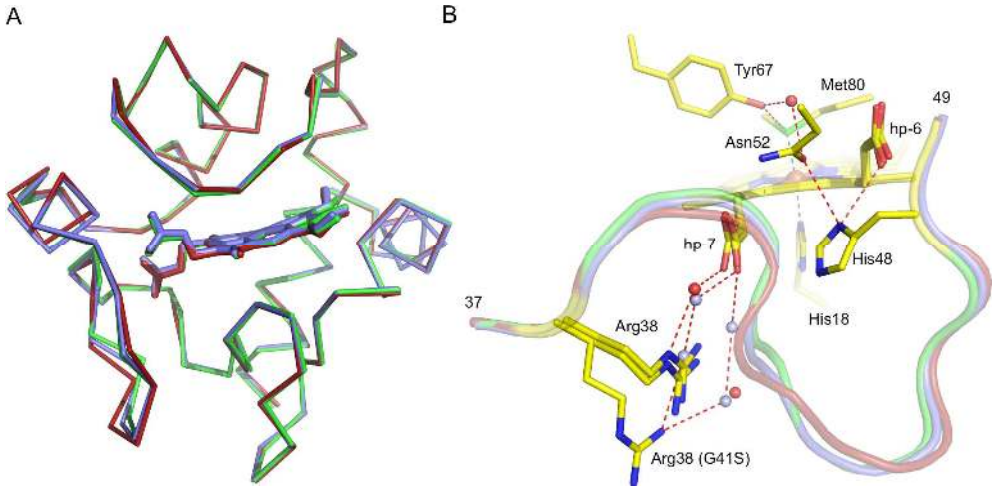

Figure 1: X-ray crystal structure of the Y48H variant of hCc. A) Ribbon representations of a Cα superposition (molecule A) of the Y48H variant (green; pdb 5O10) with the G41S variant (red; pdb 3nwv) and WT protein (blue; pdb 3zcf). The heme groups are shown in sticks. B) A cartoon and stick representation of the region between residues 37 and 49 of the WT protein (blue), the Y48H (green) and G41S (red) variants. The coordinate bonds (black dashes) of the axial His18 and Met80 ligands to the heme iron in the Y48H variant are indicated and H-bonding is represented as red dashes. The side chain position of His48, Asn52 and Tyr67 in the Y48H variant are shown together with the side chain position of Arg38 in all three structures. Water molecules are shown in red spheres for the WT and Y48H structures and in grey for the G41S variant.

therefore increases to two, with the second H-bond interaction involving the backbone amide of Thr49. A second medium length polar interaction between the Nδ1 atom of His48 and the OD1 atom of Asn52 (3.19 Å) is also noted leading to His48 communicating with the Met80 ligand through a H-bond network that extends from Asn52, involving a H_2O molecule and Tyr67 (Figure 1B). Interestingly, the Arg38 side chain in the Y48H structure is positioned as in the WT structure, with its ε-amido group coupled to heme propionate-7 via a H_2O molecule (Figure 1B). In the G41S structure the Arg38 side chain moves away from the heme propionate-7 leading to the presence of two additional H_2O molecules (Figure 1B). These waters enable the ε-amido group of Arg38 to remain coupled to the heme propionate-7 via a forked hydrogen bond network (Figure 1B).

The Y48H variant has a lower global stability than the G41S variant but a similar alkaline isomerisation pK

The Y48H variant of hCc displayed optical absorbance properties in the ferric and ferrous

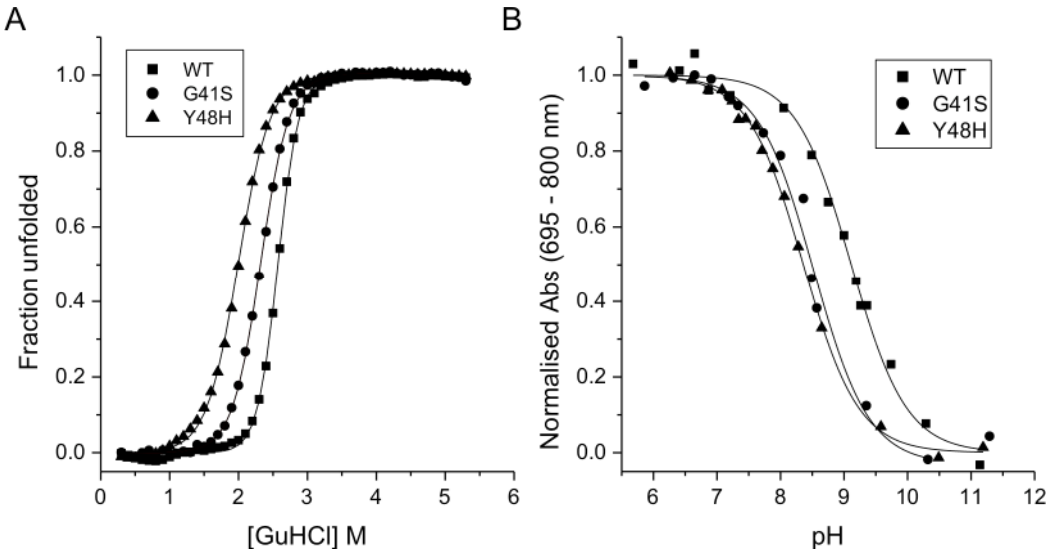

Figure 2: Global stability and pK_{695} measurement of the oxidised Y48H variant of hCc compared under identical experimental conditions with the WT protein and G41S variant. A) Plots of fraction unfolded as a function of GuHCl at pH 6.5 and 15 ^{o}C. Solid-lines are fits to the data using a two-state equilibrium unfolding equation [2], with the determined ΔG_{unf} values reported in Table 2. B) The pH dependence of the 695 nm absorbance band. Solid-lines are representative fits to the data using a one-proton equilibrium equation with pK_{695} values reported in Table 2.

oxidation states and a far-UV CD spectrum identical to that of the WT protein. Far-UV CD spectroscopy is a convenient method to determine the global stabilization of a protein through chemical denaturation studies using GuHCl as illustrated in Figure 2A. It is apparent from Figure 2A that there is a progressive loss in the cooperativity of unfolding (WT > G41S > Y48H) with the Y48H variant having the lowest global stability (ΔG_{unf}, Table 2). The *m*-value (Table 2), which is a measure of the change in hydrophobic surface area that has become desolvated upon denaturation, decreases in the order WT > G41S > Y48H, suggesting that the variants have an increasingly more compact denatured state relative to the WT protein [50]. Interestingly the K54H variant of *S. cerevisiae* iso-1 Cc stabilizes the denatured state through a His-heme loop leading to a decreased *m*-value relative to WT protein [51]. It may be that a similar effect occurs for the Y48H variant. Alternatively, the Y48H variant may simply be partially unfolded in buffer, which would also lower the *m*-value [52], with the NMR data (Fig. 6A) providing some support for this interpretation (*vide infra*).

Table 2: Summary of thermodynamic and kinetic parameters for the Y48H human ferricyt *c* variant and comparison with the WT protein and the G41S variant.

	GuHCl denaturation				Azide binding		
Protein	ΔG_{unf} (kcal mol^{-1})	m (kcal mol^{-1} M^{-1})	C_m (M)	pK_{695}	K_{app} (M)	k_1 (s^{-1})	k_{-2} (s^{-1})
Y48H	5.09 ± 0.16	2.57 ± 0.1	1.98 ± 0.05	8.4 ± 0.1	0.07 ± 0.01	125	12.1 ± 1.1
WT	10.65 ± 0.55	4.10 ± 0.25	2.60 ± 0.05	9.3 ± 0.2	0.31 ± 0.03[a]	5.77 ± 1.5[a]	3.5 ± 0.44[a]
G41S	6.75 ± 0.10	3.0 ± 0.1	2.25 ± 0.05	8.5 ± 0.2	0.11 ± 0.01[a]	45 ± 18[a]	8.9 ± 0.3[a]

[a]Data taken from reference [7].

Figure 2B shows the variation in absorbance of the 695 nm band for the oxidized Y48H variant as a function of pH compared to data for WT and the G41S variant. Although the latter pK_{695} values for the WT and G41S variant have been previously reported [27], they have been re-determined in the present study so that a true comparison under identical conditions can be made (*i.e.* in the absence of NaCl that is known to affect the pK_{695} value [53]). The bleaching of the 695 nm band is a consequence of a deprotonation event in which the axial Met80 heme ligand becomes dissociated. The apparent pK_{695} value for the Y48H variant, which was obtained from these data, is near identical to that of the G41S variant but significantly lower than that of the WT protein (Table 2). Thus, whereas the global stability for the Y48H variant is clearly decreased, the Met80-Fe(III) bond lability as determined through pK_{695} values is indistinguishable from the G41S pro-apoptotic variant.

Exogenous ligand binding reveals the pentacoordinate form of the oxidized Y48H variant is more populated than for either the G41S variant or WT hCc

To probe further variances in Met80-Fe(III) bond lability, the kinetics of N_3^- binding was

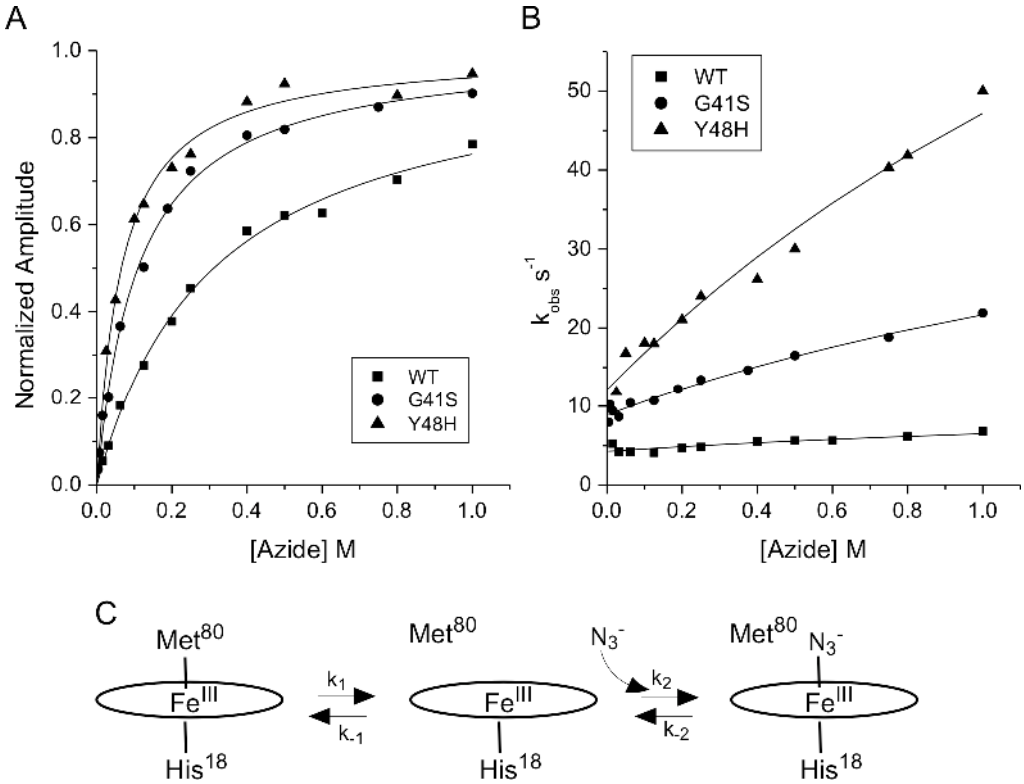

Figure 3: Azide binding to the oxidized Y48H variant of hCc variant compared with data for the WT protein and G41S variant [1] at pH 7.0 and 25 °C. A) Normalized amplitudes from the reaction time-courses obtained using stopped-flow absorption spectroscopy at 420 nm plotted against azide concentration. Data are fitted to a hyperbolic equation to yield K_{app} values reported in Table 2. B) The rate constants (k_{obs}) determined for azide binding with solid lines representative of fits to Equation 2, to give k_1 and k_{-2} reported in Table 2. C) SN_1 mechanism of azide binding to oxidized Cc.

studied using stopped-flow spectrometry. Upon mixing N_3^- with the oxidized Y48H hCc an optical transition occurred caused by the dissociation of Met80 from the heme iron and the binding of N_3^- in its place. The reaction time-course of this transition conformed to a simple exponential, as reported previously for the WT protein and the G41S variant under the same experimental conditions [1]. Over a broad range of $[N_3^-]$ the normalized amplitudes of such reaction time-courses follow a simple hyperbolic binding isotherm (Figure 3A) enabling an apparent equilibrium constant (K_{app}) for N_3^- binding to be determined. From Table 2 it is apparent that the Y48H variant binds N_3^- with a higher affinity than either the G41S variant or the WT protein. As previously reported the relationship between k_{obs} and $[N_3^-]$ under the conditions employed is almost linear [1], and is also the case here for the Y48H variant (Figure 3B). Assuming N_3^- binding to oxidized Cc is an SN_1 mechanism, in which the hexacoordinate heme form is in equilibrium with a pentacoordinate form, the latter being the form that binds N_3^- (Figure 3C), then, as outlined previously [1], Equations 1 and 2 may be

derived that describe the K_{app} and the dependence of k_{obs} for N_3^- binding as a function of [N_3^-].

$$K_{app} = K_D\left(\frac{K+1}{K}\right) \quad (1)$$

$$k_{obs} = \frac{(k_1 - k_{-2})[N_3^-]}{\left(\frac{k1+k_{-1}}{k'}\right)+[N_3^-]} + k_{-2} \quad (2)$$

In these equations, $K = k_1/k_{-1}$, where k_1 and k_{-1} are the rate constants for Met80 dissociation and association respectively and $K_D = k_{-2}/k_2$, with k_2 the pseudo-first order rate constant for N_3^- binding *i.e.* $k_2 = k'[N_3^-]$, where k' is the second order rate constant and k_{obs} is ~ k_1 at high [N_3^-]. Eq. 2 predicts that plots of k_{obs} *vs* [N_3^-] (Figure 3B) follow hyperbolae that intercept the k_{obs} axis at the value of k_{-2} (N_3^- dissociation rate constant) and plateau at k_1, the Met80 ligand dissociation rate constant. Fits of the normalized amplitude data are satisfactory and yield the values of K_{app} given in Table 2. Fitting the Y48H kinetic data to Eq. 2 presented a problem because it was not possible to explore a sufficiently high [N_3^-] where the curve is expected to reach a plateau region and thus it was difficult to discriminate between linear and hyperbolic curves. Given this we have estimated a minimum value of k_1 that provides a fit (Figure 3B), with a value (125 s^{-1}) quoted without error in Table 2, and a reliable k_{-2} value (Table 2). Nevertheless, from this estimation of k_1 it is apparent that the Y48H variant has a Met80 off-rate significantly higher than the WT protein and the G41S variant. Furthermore, Eq. 1 shows that when K < 1, as here since the concentration of the pentacoordinate species is low, then K_{app} is ~ K_D/K. With the assumption that N_3^- binding to the pentacoordinate species is not directly affected by a distant mutation in the protein then K_D will be similar for both the WT protein and the Y48H variant, so that the ratio of K_{app} values ($^{WT}K_{app}/^{Y48H}K_{app}$) reflects the ratio of K values ($^{Y48H}K/^{WT}K$). On this basis $^{Y48H}K > {}^{G41S}K > {}^{WT}K$ and thus the pentacoordinate form of Y48H variant is more populated than in either the G41S variant or the WT protein.

The population of the peroxidase active pentacoordinate form of the Y48H variant is not increased upon binding CL

The peroxidase activity of the oxidized Y48H hCc variant was compared to that of the WT protein and the G41S variant under the same experimental conditions. From the reaction time-courses given in Figure 4A it is apparent that the WT protein displays a considerable lag-phase (~ 160 s following addition of H_2O_2) in the absence of CL-containing liposomes.

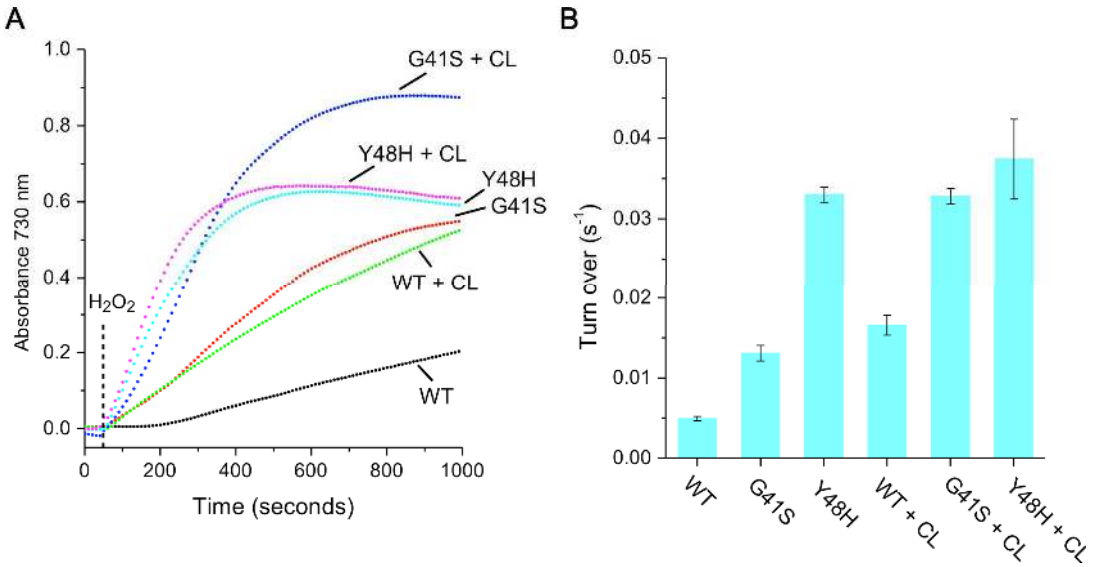

Figure 4: Peroxidase activity at pH 6.5. A) Illustrative reaction time-courses for the oxidation of ABTS in the presence of H_2O_2 with (+ CL) and without CL-containing liposomes. The vertical dashed line indicates the time point in each assay where H_2O_2 was added. B) The maximum peroxidation rates of ABTS with the various forms of ferriCc with (+ CL) and without CL-containing liposomes. The error bars are the standard error from measurements carried out in triplicate.

The lag phase is essentially absent for both the G41S and Y48H variants (Figure 4A). Peroxidase activity for the G41S variant is greater than that of the WT protein but less than that of the Y48H variant (Figure 4B). The progressive increase in peroxidase activity observed, correlates with the increase in less cooperative global unfolding (Figure 2A). In the presence of CL-containing liposomes the lag phase is now absent for the WT protein (Figure 4A) with a significant boost in peroxidase activity evident (Figure 4B). No change in peroxidase activity is observed for the Y48H variant in the presence of CL-containing liposomes, in contrast to the G41S variant where peroxidase activity is increased to a similar level as the Y48H variant (Figure 4B). The secondary increase would indicate that the binding of CL to this variant pushes the equilibrium between the hexa- and pentacoordinate heme forms further towards the latter (Figure 3C). A finding that further confirms the interpretation from the N_3^- binding kinetics, that for the Y48H variant the pentacoordinate form of the oxidized protein is energetically more favoured than it is for the G41S variant and the WT protein.

^{1}H NMR spectroscopy reveals an increase in heme pocket dynamics for the Y48H variant

The ^{1}H NMR spectrum of oxidized Cc has many resonances that are both downfield and upfield shifted due to their nuclei experiencing a hyperfine interaction from the unpaired electron on the low-spin heme iron [54]. These paramagnetic signals can inform on the electronic structure of the heme and also provide insight into heme-ligand dynamics and non-native heme-ligand states [55]. The ^{1}H NMR spectrum of the oxidized WT hCc is shown in Figure 5A with some of the upfield and downfield shifted hyperfine resonances of known assignment labelled [56, 57]. For both the WT

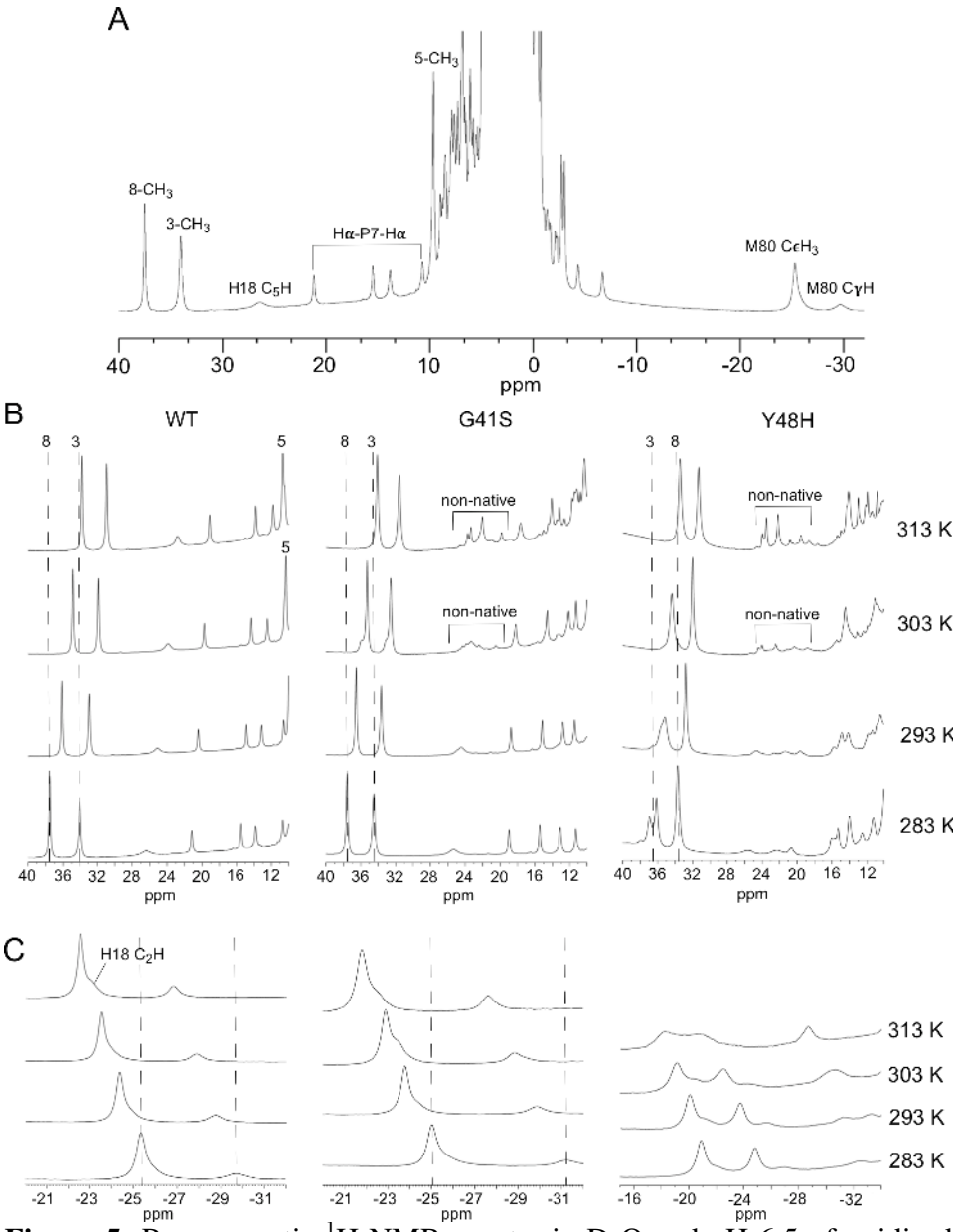

Figure 5: Paramagnetic ^{1}H NMR spectra in D_2O and pH 6.5 of oxidised hCc. A) WT Cc spectrum with several well resolved hyperfine shifted resonances arising from heme substituents and protein labelled with their assignment. B and C) Temperature dependence in the downfield and upfield regions of the spectra for the various hCc proteins. Change in chemical shift with increasing temperature for the 8- and 3-methyl heme substituents are indicated with dashed lines, along with those of the Met 80 CεH$_3$, the Met80 CγH and the His18 C_2H.

protein and G41S variant the pattern of chemical shifts for the heme-methyl signals is 8 > 3 > 5 > 1 as expected [58]. On increasing the temperature (from 283 to 313K) the hyperfine chemical shift for the 8- and 3-methyl groups of the WT protein and G41S variant display a Curie-type temperature dependence (Figure 5B), whereas the 5-methyl group displays an anti-Curie dependence. Similar temperature dependence is observed for the upfield hyperfine-shifted resonances assigned to protons of the axial His18 and Met80 heme-iron ligands (Figure 5C). For the Y48H variant the spectrum is notably different in both the upfield and downfield regions (Figure 5B and C). At 283 K there is a splitting of the hyperfine peak found at ~ 36 ppm (Figure 5B). It is known that the 3-methyl group in certain Cc's including horse heart, displays excess line broadening compared with the other heme methyl peaks at room temperature and splits into two resonances at lower temperature [59, 60]. A view consistent with exchange broadening due to rapid interconversion between heterogeneous protein environments around the 3-methyl group [60]. The splitting into two peaks at 283 K observed for the peak at ~ 36 ppm in the Y48H variant is therefore consistent with it being assigned to the 3-methyl group (Figure 5B). Raising the temperature causes the interconversion rate to increase and the two components become dynamically averaged leading to a single broadened peak. (Figure 5B). Burns and La Mar [60] showed at 298 K and pH 5.8 that the rate of the exchange process in oxidized horse heart Cc was ~10^3 s^{-1} and a similar rate for Y48H Cc at 283 K and pH 6.5 can be determined from the chemical shift difference between the heme methyl 3 resonances in the two environments (Fig. 5B). A rate considerably faster than the rate (k_1) we determine for the Met80-Fe(III) bond dissociation (Table 2), showing that the unusual dynamic process affecting heme 3-methyl is not associated with the formation of the pentacoordinate state. Furthermore, the Y48H variant alters the pattern of heme methyl chemical shifts which now become 3 > 8 > 5 > 1. Such an order of heme methyl shifts has not been previously observed in mitochondrial or bacterial oxidized Cc, where the order is either 8 > 3 > 5 > 1or 5 > 1 >8 > 3, noting that 8 is always > 3 and 5 is always > 1 in S = ½ oxidized Cc [61]. These patterns are governed by the distribution of the unpaired electron, which reflects the orientation of heme axial ligands and is largely dependent on two conformers of the Met80 side chain related through inversion of the Met thioether sulfur [58]. In this context, we note that the upfield region of the spectrum where hyperfine signals for protons of the His18 and Met80 sidechains are observed in the WT and G41S spectrum is distinctly different in the Y48H variant. Thus, although the conformation of the axial ligands is the same in the three X-ray structures the orientation of at least Met80 for the Y48H variant in solution is different. Bren *et al.* have demonstrated that fluxional

solution behaviour of the Met80 ligand is commonplace in Cc's [61]. We suggest that the altered fluxional behaviour causes a change in the magnetic susceptibility axes which perturbs the relative chemical shifts of the 3- and 8-methyl resonances [61].

Finally, we note the presence of non-native hyperfine signals in both the G41S and Y48H variants in the downfield region between 18 and 26 ppm at 303 K and above (Figure 5B). A similar set of non-native resonances has been observed for oxidized horse Cc at temperatures greater than 315 K [62], along with the WT resonances, and been assigned to the alkaline conformer with Lys and His coordination of the heme Fe(III). For the G41S and Y48H variants we suggest that as the equilibrium between the hexa- and pentacoordinate heme form is pushed further towards the latter species with increasing temperature these non-native species similarly arise from a fraction of the protein that populates the alkaline conformation. The fact that these resonances are not observed for the WT protein under similar conditions is a further indication that these pro-apoptotic variants have a more labile Met80-Fe(III) ligand. Note that the N_3^- binding study of the G41S variant [1] showed that under the conditions employed for these measurements the alkaline conformer was not significantly populated. With the higher protein concentrations and longer experimental times needed for the NMR experiments it is clear that at elevated temperatures the alkaline conformer becomes populated.

The Y48H variant has increased main-chain mobility relative to the G41S variant

To explore in more detail the dynamics of the oxidized Y48H variant, ^{15}N backbone amide H/D exchange and ^{15}N relaxation studies using NMR spectroscopy were carried out. The [^1H,^{15}N]-HSQC spectrum of the Y48H variant is shown in Figure 6A overlaid with the WT protein spectrum under identical conditions [1]. Clear differences between the two spectra exist (Figure 6A). Most notable is the significant number of backbone amide resonances absent in the Y48H spectrum compared with the WT spectrum, with a total of 64 backbone amide resonances out of a possible 99 non-proline residues being assigned (Table S1). The missing resonances are found predominately in the 40-57 Ω-loop encompassing helix-II and the 71-85 Ω-loop. At a lower magnetic field strength (500 MHz) no new peaks in the Y48H [^1H,^{15}N]-HSQC spectrum arise, which coupled with the increased line widths of the backbone amide resonances at 800 MHz is indicative of the Y48H variant having significantly greater conformational heterogeneity compared to the WT protein [1, 37].

H/D-exchange behaviour of the oxidized Y48H hCc variant was monitored and

backbone amide PFs, defined as the ratio between the observed experimental and intrinsic exchange rates (k[illegible] are influenced by H-bonding, partic[illegible]. Out of the 64 assigned backbon[illegible], leaving only 32 residues for whi[illegible] these, PFs were calculated for 29 [illegible] to calculate within the experimental [illegible] backbone amide resonances and t[illegible] be seen from the sequence depend[illegible] variant. Only the interlocking helic[illegible]-36 turn maintain various levels o[illegible] protein likely to be undergoing exten[illegible]

^{15}N relaxa[illegible] esidues, with plots of these paramet[illegible]48H variant. The average relaxatio[illegible]

^{1} an[illegible]

= 0.

WT [illegible]

and [illegible]

NOI

Fi

mot[illegible]

ox[illegible]

the[illegible]

exce[illegible]

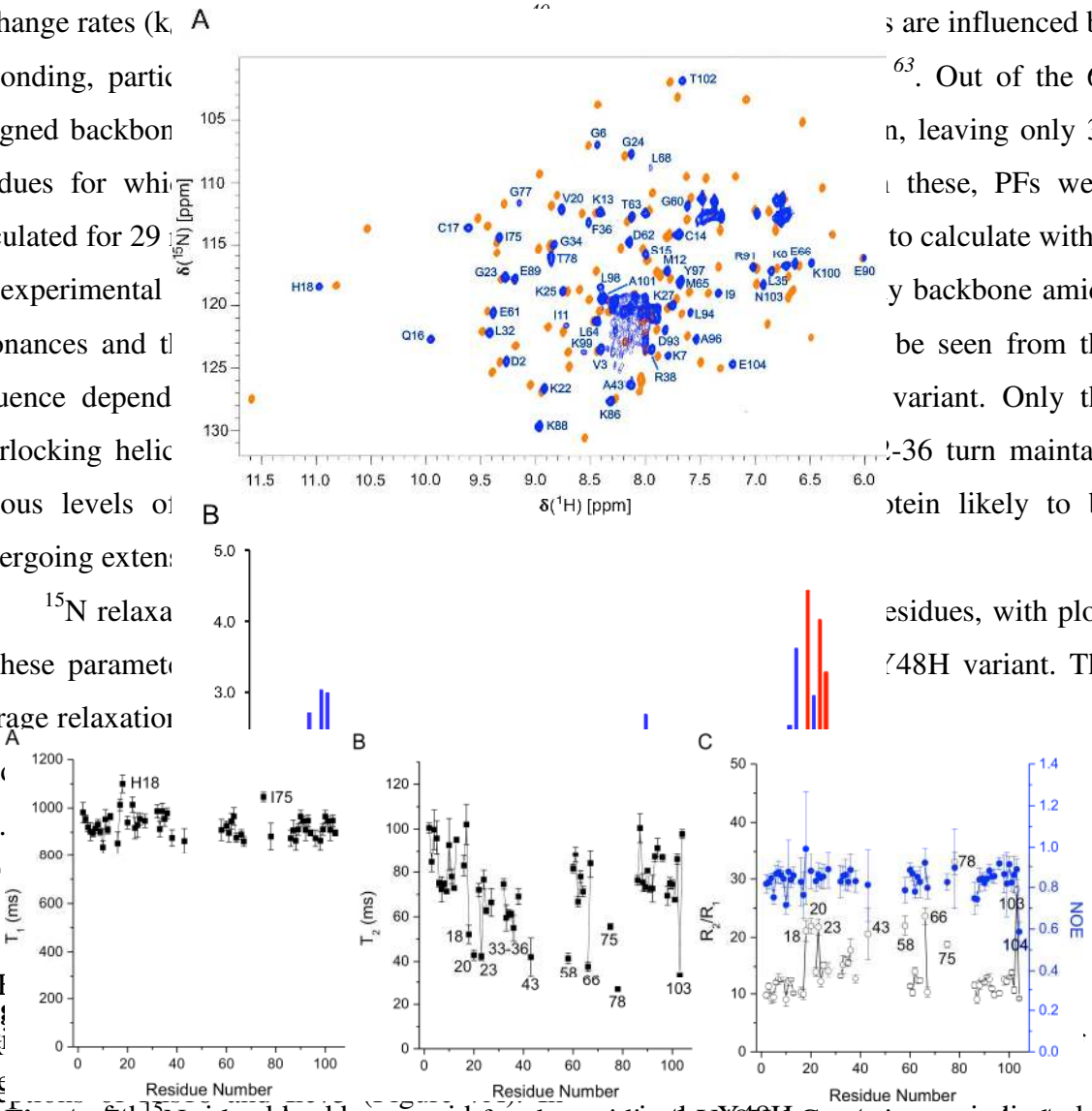

Figure 7: ^{15}N relaxation parameters for the oxidized Y48H hCP variant acquired at 800 MHz and 288 K. A) T_1 and B) T_2 times plotted against residue number. C) R_2/R_1 ratio (blue circles) and ^{15}N-{^{1}H} NOE (blue circles) plotted against residue number. For the PFs that could be calculated, 3 residues undergo fast exchange (logPF ≤ 1), 13 medium (1 < logPF ≤ 2), 10 slow (2 < logPF) and 3 extremely slow-exchange (residual proton occupancy > 80 % after ~ 138 h corresponding to exchange rates < 0.003 h^{-1}, shown in red). Secondary structure (α-helix) is indicated by the bottom red squares with the 5 α-helices numbered I-V, while red squares above represent Pro residues. Unassigned and fast-exchanging residues are indicated in dark blue and yellow squares, respectively. Residues for which PFs could not be calculated due to the slowness of the exchange are indicated with black squares (3 residues).

for most of the assigned backbone amide resonances in the Y48H spectrum are indicated in contrast, the T$_1$ plot reveals a significant number [illegible] of residues that deviate below the average [illegible] (Figure 7B), probably reflecting contributions to relaxation from slower conformational exchange equilibria. A useful indicator to identify residues experiencing chemical exchange is a plot of the R_2/R_1 ratio (Figure 7C). Despite the smaller size of the relaxation data set for the Y48H variant (55 residues) compared to the G41S variant (92 residues) [7], a similar pattern of residues experiencing slow conformational exchange emerges (*i.e.* 14-36, 40-57 and 71-85 Ω-loops) and is also in keeping with the regions experiencing rapid H/D-exchange (Figure 6B).

DISCUSSION

The past two decades of Cc research has placed this essential redox protein firmly into the category of a moonlighting or EMF protein [64]. For Cc to have a peroxidatic moonlighting function, then access to an alternative structural state or conformer is required. Such a form could come about because Cc binding of CL results in a conformational change to create the peroxidatic state or because the ground-state structure is in equilibrium with one or more minor higher-energy forms of different structure and CL binding displaces the equilibrium by binding preferentially to a higher-energy state. We have shown for the pro-apoptotic G41S variant of hCc enhanced conformational dynamics of the 40-57 Ω-loop exists and is directly linked to the dissociation of the Met80-Fe(III) ligand in the 71-85 Ω-loop. Cross-talk between Ω-loop results in an increased population of the peroxidatic pentacoordinate state [1], which under healthy conditions aids in controlling levels of reactive oxygen species (ROS), but during the early phase of mitochondrial apoptosis results in Cc peroxidising the membrane lipid CL. Furthermore, once released from the mitochondrion Cc has also been implicated in the peroxidation of the plasma membrane lipid phosphatidylserine [65]. The second thrombocytopenia 4 associated mutation of hCc to be discovered was the Y48H variant [25] and is also located within the 40-57 Ω-loop. In Cc evolution, this is the least conserved Ω-loop and has the lowest free energy of the five-cooperative folding/unfolding units (foldons) assigned in Cc [66, 67]. Perhaps not surprisingly therefore, the Y48H variant displays enhanced mobility and dynamics. However, it is apparent that the dynamics, both local and global, are further enhanced in the Y48H variant compared to the G41S variant. Such behaviour is revealed by ~ 35 % of backbone amide resonances for the Y48H variant remaining unassigned due to their absence in the ^{1}H-^{15}N HSQC spectrum compared to 2 and 6 % for the WT protein and G41S variant, respectively, under identical conditions. Except for Ala43 the whole of the 40-57 Ω-loop is unassigned, along with the latter half (residues 79-85) of the 71-85 Ω-loop, the second least stable foldon [67], housing the Met80-Fe(III) ligand. These missing resonances in the Y48H variant are a likely consequence of a decreased T_2 resulting from exchange between different conformations. Although we cannot demonstrate unequivocally from direct NMR measurements, because of the missing resonances, that the Y48H variant has enhanced dynamics on the μs-ms timescale (*i.e.* compute R_{ex} terms), it is apparent for the resonances which allow for an amide H/D exchange PF to be calculated (*i.e.* those from the N- and C-terminal helices, the end of the 14-36 Ω-loop and some of helix 3) that these are generally smaller for the Y48H variant than for the other proteins [1]. Visualization of the spread in increasing dynamics can be appreciated from mapping amide

H/D exchange data onto the respective Cc X-ray structures (Figure 8A). From this it is apparent that helices I, III and V for all proteins maintain similar H/D profiles with the mutations clearly resulting in more rapid exchange and thus enhanced dynamics (WT < G41S < Y48H) in the 40-57 and 71-85 Ω-loops, as well as helix II (Figure 8A).

Englander and colleagues have elegantly determined how Cc folds through uncovering its foldon substructure [66, 67]. Of the five foldons, the two with the lowest stability are the 40-57 and 71-85 Ω loops [5, 68]. The correlation between the conformational dynamics linking the G41S and Y48H mutations with the displacement of the Met80 ligand and the energetics of

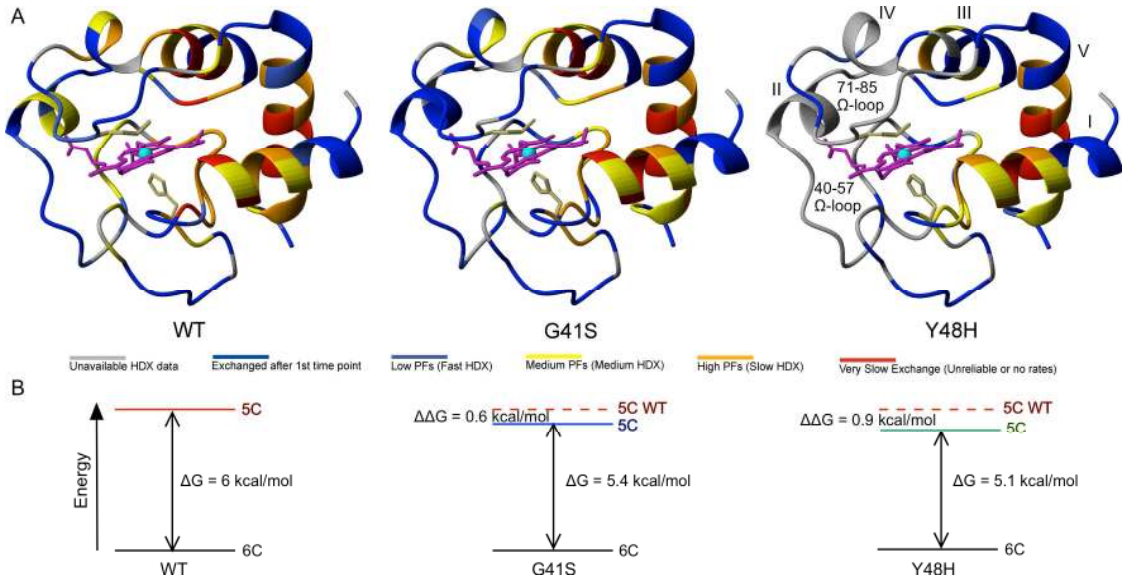

Figure 8: Dynamics in the hCc variants attributed to causing thrombocytopenia 4. A) PF mapping onto the respective X-ray structures of hCc, with PFs colour coded as indicated. The data for the ferric WT protein and ferric G41S variant are taken from [1] with the data for the Y48H variant taken form the LogP plot in Figure 6B. The heme and axial ligands are shown in stick and helices labelled I to V. B) Energy diagrams illustrating the calculated differences in free energy change (ΔΔG) between the pentacoordinate forms in the various species derived from $\Delta G = -RT\ln({}^{WT}K_{app}/{}^{variant}K_{app})$ from N_3^- binding kinetics. The ΔG for the WT protein is based on Hu *et al.* [5].

the foldon substructure is striking. Making the assumption that the pentacoordinate state of oxidized Cc is equivalent to the partially unfolded form, with the two lowest energy foldons unfolded, placs the pentacoordinate state at 6 kcal/mol above the ground state structure, based on the analyses of Hu *et al.* [5] and assuming the energetics of horse Cc are the same as those of hCc. From $\Delta G = -RT\ln({}^{WT}K_{app}/{}^{Y48H}K_{app})$ (determined from the kinetics of N_3^- binding) the relative ΔΔG of the pentacoordinate state of the various Cc forms may be calculated as illustrated by the energy level diagrams in Figure 8B, since, as noted earlier, the ratio ${}^{WT}K_{app}/{}^{Y48H}K_{app}$ reflects the ratio of equilibrium constants for dissociation and re-association

of the Met80 ligand ($^{Y48H}K/^{WT}K$), with the assumption that the free energy of the ground state is the same for both the variant and the WT protein. Thus, as illustrated in Figure 8B the pentacoordinate form is 0.9 kcal/mol and 0.6 kcal/mol lower in energy than the WT protein for the Y48H and G41S variants, respectively, than for the WT protein. Each kcal/mol change denotes a ~ 5-fold change in the equilibrium constant governing the distribution between the hexa- and pentacoordinated forms. If the minor component in such an equilibrium, here the pentacoordinated form, plays a significant mechanistic role, this mean that for a kcal/mol change in stability the concentration of this minor component increases ~ 5-fold. Our proposal that the G41S and Y48H variants cause small changes in the oxidized hCc energy landscape should be considered alongside the recent finding that the Fe(III)-S(Met) bond of Cc is weak and requires constraints imposed by the protein structure, such as extensive H-bonding of neighbouring residues, to be maintained under physiological conditions [69, 70]. Stabilisation of a weak bond by a protein structure is an example of entasis, originally proposed to account for some of the apparently unusual properties of metalloproteins by suggesting that the metal centre 'constituted an energetically poised domain' [71], and Mara *et al.* [70] have determined that the protein entatic contribution to the Fe(III)-S(Met) bond is ~ 4 kcal/mol. It is readily appreciated therefore that small changes in the energy landscape can have mechanistic effects and contribute to this moonlighting function of Cc.

From the peroxidase assays it is particularly noteworthy that the turnover of H_2O_2 by the Y48H variant is not boosted in the presence of CL-liposomes, as is the case for the WT protein and the G41S variant (Figure 4B). An absence of a CL boosting effect for G41 variants has been reported by others [28] and thus contrasts with both our previous observations using an Amplex red assay [27] and in the present study using ABTS. Our findings that there is a boost in peroxidase activity for the G41S variant in the presence of CL-liposomes are wholly consistent with our dynamic appraisal of these two variants. The Y48H variant is more dynamic than G41S variant with the equilibrium between the hexa- and pentacoordinate species no longer rate-limiting in this peroxidase assay for the Y48H variant as the concentration of the reactive pentacoordinate form is further increased (Figure 8B).

Access of small molecules such as H_2O_2 to the heme has been suggested to occur through a gating motion of Arg38 based on its side chain repositioning in the G41S variant creating a 'channel' to enable H_2O molecules to access the heme [27, 44]. A subsequent X-ray structure of the K72A variant of *Saccharomyces cerevisiae* Cc revealed the Met80 ligand to be dissociated from the heme iron and the Arg38 side chain positioned in an 'out' position as

observed in the G41S structure [72]. A network of H-bonded H_2O molecules connects the Met80 side of the heme to the bulk solvent in the K72A structure [72]. Repositioning of Arg38 thus causes perturbations to the environment of the heme propionate substituent at position 7 and may be considered to influence the dynamics of the 40-57 Ω-loop, which is linked to the dissociation of the Met80 ligand [1, 27]. However, we note that in the X-ray structure of the Y48H variant the Arg38 side chain is in the same position as in the WT protein (Figure 1B). Comparison of the G41S and Y48H X-ray structures reveals that the introduction of a Ser or His at positions 41 and 48, respectively, creates the opportunity for both side chains to form a H-bond to the side chain of Asn52 (Figure 1B). The latter communicates with the Met80 ligand through further H-bond interactions (Figure 1B). Thus, we propose that there are two possible conformational routes by which dynamical changes at the base of the heme could be communicated to the Met80 ligand. Indeed, the literature contains many reports showing that the 40-57 Ω-loop and heme crevice have an important conformational linkage, though this was not something always recognised at the time. For example, Robinson *et al.* [73], based on incomplete NMR data showed that residues in the 40-57 Ω-loop rapidly interconverted between different local conformational states under native conditions. Our suggested role of Asn52 is consistent with observations of Schejter *et al.* [74], who present data on CN^- binding to a N52I variant of *S. cerevisiae* Cc, that is indicative of a reduced population of the pentacoordinate form. A linkage has also been discussed in connection with the alkaline isomerisation of oxidized Cc [75] and is supported by the NMR structure of a triple variant of *S. cerevisiae* ferric Cc engineered to stabilize the alkaline conformer [76]. The triple variant structure showed that the 71-85 Ω loop with the displaced Met80 ligand and the 40-57 Ω-loop were the most perturbed feature compared with the WT structure. [76]

Recent studies have highlighted that Cc function can be governed by phosphorylation, where it regulates the electron-transport chain flux preventing hyperpolarization of the mitochondrial membrane potential, a known cause of ROS and trigger of apoptosis [77, 78]. Three phosphorylation sites on isolates of bovine Cc have been identified from different tissues and include Thr28, Tyr48 and Tyr97 [79-81]. Considering the reported pro-apoptotic behavior of the Y48H variant [25], it is interesting to note that one of the phosphorylation sites is Tyr48, which when phosphorylated abolishes the capability to trigger apoptosis at the apoptosome level [82-84]. A recent study has characterized a Tyr48 phosphomimetic (designated Tyr48p) using a non-native amino acid to assess the effect of phosphorylation at this position on the hCc structure [84]. Structural studies were conducted with the ferrous form, which is the

heme oxidation state that donates an electron to Cc oxidase [12], and not the state that gives rise to the peroxidatic pentacoordinate form, central to our work. The WT reduced Cc has a more rigid structure than its oxidized counterpart, and an equilibrium between the Met80-on and Met80-off has not been detected under non-apoptosis physiological conditions [85]. Despite this, the dynamics on the μs-ms timescale for the reduced Tyr48p Cc showed increased mobility compared to the WT protein, particularly, in the 40-57 Ω-loop, but with an overall increase significantly lower than the G41S and Y48H variants in their oxidized forms. Furthermore, an increase in mobility for the Tyr48p reduced Cc was also observed for residues 75-78 in the 71-85 Ω-loop again highlighting the link between the 40-57 Ω-loop and the Met80 ligand. In the ferric state the Tyr48p exhibits a 3-fold increase in peroxidase activity relative to the WT protein [84], in contrasts to the Y48H variant where a 7-fold increase in activity is observed (Figure 4B). In the presence of CL-liposomes the Tyr48p displays a 7-fold boost in peroxidase activity relative to the WT protein and thus on a par with the Y48H variant in the absence or presence of CL (Figure 4B). Therefore, these data suggest that the equilibrium constant between the hexacoordinate and pentacoordinate heme forms (Figure 3C) favours the hexacoordinate form in Tyr48p relative to the Y48H variant, enabling CL to further regulate the activity of the phosphorylated protein which may have consequences for pro- and anti-apoptotic behaviour insofar as we have shown that the pentacoordinate heme form is critical for this.

In conclusion, we have shown that the naturally occurring Y48H variant of hCc in its oxidized heme state is more peroxidatic than either the WT protein or the G41S variant that is also implicated in thrombocytopenia. The dynamic fluctuations in the 40-57 Ω-loop resulting in cross-talk with the 71-85 Ω-loop containing the Met80 ligand are further amplified in the Y48H variant. Consequently, the Y48H protein has intrinsic peroxidase activity that is no longer enhanced in the presence of CL because of the increased population of an excited pentacoordinate heme state structure lying close in energy to the ground state Met80 coordinated structure. These finding underpins our proposal that the switch in function of the moonlighting Cc from electron-transfer to peroxidase is, at least partly, a result of its pre-existing conformational equilibrium involving an excited pentacoordinate state. A third naturally occurring variant, A51V, also implicated in thrombocytopenia has not yet been characterized. Owing to the location of the variant on the 40-57 Ω-loop it may be predicted to have similar traits to the G41S and Y48H variants and it will therefore be interesting to

discover where this variant is located within the dynamic window (WT < G41S < Y48H) that has emerged from the studies so far.

ACKNOWLEDGEMENTS

Our work was supported by a Leverhulme Trust project grant (RPG-2013-164) to J.A.R.W. and a Leverhulme Trust emeritus fellowship (EM-2014-088) to G.R.M. Access to the Swiss Light Source was via Long-Term award 20160704 to MAH.

SUPPORTING INFORMATION

A supporting information Table is available, Table S1 that reports on the chemical shift assignments and the H/D exchange rates (k_{ex}), calculated protection factors (log P), free energy of exchange (ΔG_{ex}) and proton occupancy values (Occ) for oxidized Y48H hCc (pH 6.5 and 288 K).

REFERENCES

[1] Karsisiotis, A. I., Deacon, O. M., Wilson, M. T., Macdonald, C., Blumenschein, T. M., Moore, G. R., and Worrall, J. A. (2016) Increased dynamics in the 40-57 Ω-loop of the G41S variant of human cytochrome c promote its pro-apoptotic conformation, *Sci Rep 6*, 30447.

[2] Santoro, M. M., and Bolen, D. W. (1992) A test of the linear extrapolation of unfolding free energy changes over an extended denaturant concentration range, *Biochemistry 31*, 4901-4907.

[3] Henderson, B., and Martin, A. C. (2014) Protein moonlighting: a new factor in biology and medicine, *Biochem Soc Trans 42*, 1671-1678.

[4] Jeffery, C. J. (2014) An introduction to protein moonlighting, *Biochem Soc Trans 42*, 1679-1683.

[5] Hu, W., Kan, Z. Y., Mayne, L., and Englander, S. W. (2016) Cytochrome c folds through foldon-dependent native-like intermediates in an ordered pathway, *Proc Natl Acad Sci U S A 113*, 3809-3814.

[6] Jeffery, C. J. (1999) Moonlighting proteins, *Trends Biochem Sci 24*, 8-11.

[7] Chapple, C. E., Robisson, B., Spinelli, L., Guien, C., Becker, E., and Brun, C. (2015) Extreme multifunctional proteins identified from a human protein interaction network, *Nat Commun 6*, 7412.

[8] Chapple, C. E., and Brun, C. (2015) Redefining protein moonlighting, *Oncotarget 6*, 16812-16813.

[9] Bryngelson, J. D., Onuchic, J. N., Socci, N. D., and Wolynes, P. G. (1995) Funnels, pathways, and the energy landscape of protein folding: a synthesis, *Proteins 21*, 167-195.

[10] Henzler-Wildman, K., and Kern, D. (2007) Dynamic personalities of proteins, *Nature 450*, 964-972.

[11] Baldwin, A. J., and Kay, L. E. (2009) NMR spectroscopy brings invisible protein states into focus, *Nat Chem Biol 5*, 808-814.

[12] Ferguson-Miller, S., and Babcock, G. T. (1996) Heme/Copper Terminal Oxidases, *Chem Rev 96*, 2889-2908.
[13] Ow, Y. P., Green, D. R., Hao, Z., and Mak, T. W. (2008) Cytochrome c: functions beyond respiration, *Nat Rev Mol Cell Biol 9*, 532-542.
[14] Huttemann, M., Pecina, P., Rainbolt, M., Sanderson, T. H., Kagan, V. E., Samavati, L., Doan, J. W., and Lee, I. (2011) The multiple functions of cytochrome c and their regulation in life and death decisions of the mammalian cell: From respiration to apoptosis, *Mitochondrion 11*, 369-381.
[15] Kagan, V. E., Tyurin, V. A., Jiang, J., Tyurina, Y. Y., Ritov, V. B., Amoscato, A. A., Osipov, A. N., Belikova, N. A., Kapralov, A. A., Kini, V., Vlasova, II, Zhao, Q., Zou, M., Di, P., Svistunenko, D. A., Kurnikov, I. V., and Borisenko, G. G. (2005) Cytochrome c acts as a cardiolipin oxygenase required for release of proapoptotic factors, *Nat Chem Biol 1*, 223-232.
[16] Wang, X. (2001) The expanding role of mitochondria in apoptosis, *Genes Dev 15*, 2922-2933.
[17] Bruey, J. M., Ducasse, C., Bonniaud, P., Ravagnan, L., Susin, S. A., Diaz-Latoud, C., Gurbuxani, S., Arrigo, A. P., Kroemer, G., Solary, E., and Garrido, C. (2000) Hsp27 negatively regulates cell death by interacting with cytochrome c, *Nat Cell Biol 2*, 645-652.
[18] Boehning, D., Patterson, R. L., Sedaghat, L., Glebova, N. O., Kurosaki, T., and Snyder, S. H. (2003) Cytochrome c binds to inositol (1,4,5) trisphosphate receptors, amplifying calcium-dependent apoptosis, *Nat Cell Biol 5*, 1051-1061.
[19] Gonzalez-Arzola, K., Diaz-Moreno, I., Cano-Gonzalez, A., Diaz-Quintana, A., Velazquez-Campoy, A., Moreno-Beltran, B., Lopez-Rivas, A., and De la Rosa, M. A. (2015) Structural basis for inhibition of the histone chaperone activity of SET/TAF-Ibeta by cytochrome c, *Proc Natl Acad Sci U S A 112*, 9908-9913.
[20] Cummings, C., Walder, J., Treeful, A., and Jemmerson, R. (2006) Serum leucine-rich alpha-2-glycoprotein-1 binds cytochrome c and inhibits antibody detection of this apoptotic marker in enzyme-linked immunosorbent assay, *Apoptosis 11*, 1121-1129.
[21] Yu, T., Wang, X., Purring-Koch, C., Wei, Y., and McLendon, G. L. (2001) A mutational epitope for cytochrome C binding to the apoptosis protease activation factor-1, *J Biol Chem 276*, 13034-13038.
[22] Speck, S. H., Ferguson-Miller, S., Osheroff, N., and Margoliash, E. (1979) Definition of cytochrome c binding domains by chemical modification: kinetics of reaction with beef mitochondrial reductase and functional organization of the respiratory chain, *Proc Natl Acad Sci U S A 76*, 155-159.
[23] Rieder, R., and Bosshard, H. R. (1980) Comparison of the binding sites on cytochrome c for cytochrome c oxidase, cytochrome bc1, and cytochrome c1. Differential acetylation of lysyl residues in free and complexed cytochrome c, *J Biol Chem 255*, 4732-4739.
[24] Morison, I. M., Cramer Borde, E. M., Cheesman, E. J., Cheong, P. L., Holyoake, A. J., Fichelson, S., Weeks, R. J., Lo, A., Davies, S. M., Wilbanks, S. M., Fagerlund, R. D., Ludgate, M. W., da Silva Tatley, F. M., Coker, M. S., Bockett, N. A., Hughes, G., Pippig, D. A., Smith, M. P., Capron, C., and Ledgerwood, E. C. (2008) A mutation of human cytochrome c enhances the intrinsic apoptotic pathway but causes only thrombocytopenia, *Nat Genet 40*, 387-389.
[25] De Rocco, D., Cerqua, C., Goffrini, P., Russo, G., Pastore, A., Meloni, F., Nicchia, E., Moraes, C. T., Pecci, A., Salviati, L., and Savoia, A. (2014) Mutations of cytochrome c identified in patients with thrombocytopenia THC4 affect both apoptosis and cellular bioenergetics, *Biochim Biophys Acta 1842*, 269-274.

[26] Johnson, B., Lowe, G. C., Futterer, J., Lordkipanidze, M., MacDonald, D., Simpson, M. A., Sanchez-Guiu, I., Drake, S., Bem, D., Leo, V., Fletcher, S. J., Dawood, B., Rivera, J., Allsup, D., Biss, T., Bolton-Maggs, P. H., Collins, P., Curry, N., Grimley, C., James, B., Makris, M., Motwani, J., Pavord, S., Talks, K., Thachil, J., Wilde, J., Williams, M., Harrison, P., Gissen, P., Mundell, S., Mumford, A., Daly, M. E., Watson, S. P., and Morgan, N. V. (2016) Whole exome sequencing identifies genetic variants in inherited thrombocytopenia with secondary qualitative function defects, *Haematologica 101*, 1170-1179.

[27] Rajagopal, B. S., Edzuma, A. N., Hough, M. A., Blundell, K. L., Kagan, V. E., Kapralov, A. A., Fraser, L. A., Butt, J. N., Silkstone, G. G., Wilson, M. T., Svistunenko, D. A., and Worrall, J. A. (2013) The hydrogen-peroxide-induced radical behaviour in human cytochrome c-phospholipid complexes: implications for the enhanced pro-apoptotic activity of the G41S mutant, *Biochem J 456*, 441-452.

[28] Josephs, T. M., Morison, I. M., Day, C. L., Wilbanks, S. M., and Ledgerwood, E. C. (2014) Enhancing the peroxidase activity of cytochrome c by mutation of residue 41: implications for the peroxidase mechanism and cytochrome c release, *Biochem J 458*, 259-265.

[29] Mason, J. M., Bendall, D. S., Howe, C. J., and Worrall, J. A. (2012) The role of a disulfide bridge in the stability and folding kinetics of Arabidopsis thaliana cytochrome c(6A), *Biochim Biophys Acta 1824*, 311-318.

[30] Kabsch, W. (2010) XDS, *Acta Cryst D, 66*, 125-132.

[31] Evans, P. R., and Murshudov, G. N. (2013) How good are my data and what is the resolution?, *Acta Cryst D 69*, 1204-1214.

[32] McCoy, A. J., Grosse-Kunstleve, R. W., Adams, P. D., Winn, M. D., Storoni, L. C., and Read, R. J. (2007) Phaser crystallographic software, *J Appl Crystallogr 40*, 658-674.

[33] Murshudov, G. N., Vagin, A. A., and Dodson, E. J. (1997) Refinement of macromolecular structures by the maximum-likelihood method, *Acta Cryst D, 53*, 240-255.

[34] Emsley, P., and Cowtan, K. (2004) Coot: model-building tools for molecular graphics, *Acta Cryst D 60*, 2126-2132.

[35] Davis, I. W., Leaver-Fay, A., Chen, V. B., Block, J. N., Kapral, G. J., Wang, X., Murray, L. W., Arendall, W. B., 3rd, Snoeyink, J., Richardson, J. S., and Richardson, D. C. (2007) MolProbity: all-atom contacts and structure validation for proteins and nucleic acids, *Nucleic Acids Res 35*, W375-383.

[36] Krissinel, E. (2012) Enhanced fold recognition using efficient short fragment clustering, *J Mol Biochem 1*, 76-85.

[37] Karsisiotis, A. I., Deacon, O. M., Rajagopal, B. S., Macdonald, C., Blumenschein, T. M., Moore, G. R., and Worrall, J. A. (2015) Backbone resonance assignments of ferric human cytochrome c and the pro-apoptotic G41S mutant in the ferric and ferrous states, *Biomol NMR Assign 9*, 415-419.

[38] Vranken, W. F., Boucher, W., Stevens, T. J., Fogh, R. H., Pajon, A., Llinas, M., Ulrich, E. L., Markley, J. L., Ionides, J., and Laue, E. D. (2005) The CCPN data model for NMR spectroscopy: development of a software pipeline, *Proteins 59*, 687-696.

[39] Goddard, T. D., and Kneller, D. G. (2008) SPARKY 3, *University of California, San Francisco*.

[40] Bai, Y., Milne, J. S., Mayne, L., and Englander, S. W. (1993) Primary structure effects on peptide group hydrogen exchange, *Proteins 17*, 75-86.

[41] Hoshino, M., Katou, H., Yamaguchi, K.-I., and Goto, Y. (2007) Dimethylsulfoxide-quenched hydrogen/deuterium exchange method to study amyloid fibril structure, *Biochim Biophys Acta 1768*, 1886-1899.

[42] Palmer, A. G., Rance, M., and Wright, P. E. (1991) Intramolecular Motions of a Zinc Finger DNA-Binding Domain from Xfin Characterized by Proton-Detected Natural Abundance C-12 Heteronuclear Nmr-Spectroscopy, *J Am Chem Soc 113*, 4371-4380.
[43] Delaglio, F., Grzesiek, S., Vuister, G. W., Zhu, G., Pfeifer, J., and Bax, A. (1995) NMRPipe: a multidimensional spectral processing system based on UNIX pipes, *J Biomol NMR 6*, 277-293.
[44] Liptak, M. D., Fagerlund, R. D., Ledgerwood, E. C., Wilbanks, S. M., and Bren, K. L. (2011) The Proapoptotic G41S Mutation to Human Cytochrome c Alters the Heme Electronic Structure and Increases the Electron Self-Exchange Rate, *J Am Chem Soc 133*, 1153-1155.
[45] Zeldin, O. B., Gerstel, M., and Garman, E. F. (2013) RADDOSE-3D: time- and space-resolved modelling of dose in macromolecular crystallography, *J Appl Crystallogr 46*, 1225-1230.
[46] Beitlich, T., Kuhnel, K., Schulze-Briese, C., Shoeman, R. L., and Schlichting, I. (2007) Cryoradiolytic reduction of crystalline heme proteins: analysis by UV-Vis spectroscopy and X-ray crystallography, *J Synchro Rad 14*, 11-23.
[47] Kekilli, D., Moreno-Chicano, T., Chaplin, A. K., Horrell, S., Dworkowski, F. S. N., Worrall, J. A. R., Strange, R. W., and Hough, M. A. (2017) Photoreduction and validation of haem-ligand intermediate states in protein crystals by in situ single-crystal spectroscopy and diffraction, *IUCrJ 4*, 263-270.
[48] Takano, T., and Dickerson, R. E. (1981) Conformation change of cytochrome c. II. Ferricytochrome c refinement at 1.8 A and comparison with the ferrocytochrome structure, *J Mol Biol 153*, 95-115.
[49] Brayer, G. D., and Murphy, M. P. (1996) Structural studies of eukaryotic cytochromes c, In *Cytochorme c: A multidiciplinary approach* (Scott, R. A., and Mauk, A. G., Eds.) 1 ed., pp 103-166, University Science Books, Sausalito, California.
[50] Shortle, D. (1995) Staphylococcal nuclease: a showcase of m-value effects, *Advances in protein chemistry 46*, 217-247.
[51] Hammack, B. N., Smith, C. R., and Bowler, B. E. (2001) Denatured state thermodynamics: residual structure, chain stiffness and scaling factors, *J Mol Biol 311*, 1091-1104.
[52] Godbole, S., Dong, A., Garbin, K., and Bowler, B. E. (1997) A lysine 73-->histidine variant of yeast iso-1-cytochrome c: evidence for a native-like intermediate in the unfolding pathway and implications for m value effects, *Biochemistry 36*, 119-126.
[53] Rosell, F. I., Ferrer, J. C., and Mauk, A. G. (1998) Proton-linked protein conformational switching: Definition of the alkaline conformational transition of yeast iso-1-ferricytochrome c, *J Am Chem Soc 120*, 11234-11245.
[54] Wuthrich, K. (1969) High-resolution proton nuclear magnetic resonance spectroscopy of cytochrome, *Proc Natl Acad Sci U S A 63*, 1071-1078.
[55] Ubbink, M., Worrall, J. A., Canters, G. W., Groenen, E. J., and Huber, M. (2002) Paramagnetic resonance of biological metal centers, *Annu Rev Biophys Biomol Struct 31*, 393-422.
[56] Santos, H., and Turner, D. L. (1987) Proton NMR studies of horse ferricytochrome c. Completion of the assignment of the well resolved hyperfine shifted resonances, *FEBS Lett 226*, 179-185.
[57] Feng, Y. Q., Roder, H., and Englander, S. W. (1990) Assignment of paramagnetically shifted resonances in the ^{1}H NMR spectrum of horse ferricytochrome c, *Biophys J 57*, 15-22.

[58] Senn, H., and Wuthrich, K. (1985) Amino acid sequence, haem-iron co-ordination geometry and functional properties of mitochondrial and bacterial c-type cytochromes, *Q Rev Biophys 18*, 111-134.
[59] Burns, P. D., and Lamar, G. N. (1979) Detection of Localized Conformational Flexibility in Horse Heart Cytochrome-C by Proton Nuclear Magnetic-Resonance, *J Amer Chem Soc 101*, 5844-5846.
[60] Burns, P. D., and La Mar, G. N. (1981) Characterization of conformational heterogeneity in the heme pocket of ferricytochrome c using high field proton nuclear magnetic resonance spectroscopy, *J Biol Chem 256*, 4934-4939.
[61] Zhong, L., Wen, X., Rabinowitz, T. M., Russell, B. S., Karan, E. F., and Bren, K. L. (2004) Heme axial methionine fluxionality in Hydrogenobacter thermophilus cytochrome c552, *Proc Natl Acad Sci U S A 101*, 8637-8642.
[62] Angstrom, J., Moore, G. R., and Williams, R. J. P. (1982) The Magnetic-Susceptibility of Ferricytochrome-C, *Biochim Biophys Acta 703*, 87-94.
[63] Englander, S. W., and Kallenbach, N. R. (1983) Hydrogen-Exchange and Structural Dynamics of Proteins and Nucleic-Acids, *Q Revs Biophys 16*, 521-655.
[64] Hannibal, L., Tomasina, F., Capdevila, D. A., Demicheli, V., Tortora, V., Alvarez-Paggi, D., Jemmerson, R., Murgida, D. H., and Radi, R. (2016) Alternative Conformations of Cytochrome c: Structure, Function, and Detection, *Biochemistry 55*, 407-428.
[65] Bayir, H., Fadeel, B., Palladino, M. J., Witasp, E., Kurnikov, I. V., Tyurina, Y. Y., Tyurin, V. A., Amoscato, A. A., Jiang, J., Kochanek, P. M., DeKosky, S. T., Greenberger, J. S., Shvedova, A. A., and Kagan, V. E. (2006) Apoptotic interactions of cytochrome c: redox flirting with anionic phospholipids within and outside of mitochondria, *Biochim Biophys Acta 1757*, 648-659.
[66] Krishna, M. M., Lin, Y., Rumbley, J. N., and Englander, S. W. (2003) Cooperative omega loops in cytochrome c: role in folding and function, *J Mol Biol 331*, 29-36.
[67] Krishna, M. M., Maity, H., Rumbley, J. N., Lin, Y., and Englander, S. W. (2006) Order of steps in the cytochrome c folding pathway: evidence for a sequential stabilization mechanism, *J Mol Biol 359*, 1410-1419.
[68] Maity, H., Maity, M., Krishna, M. M., Mayne, L., and Englander, S. W. (2005) Protein folding: the stepwise assembly of foldon units, *Proc Natl Acad Sci U S A 102*, 4741-4746.
[69] Kroll, T., Hadt, R. G., Wilson, S. A., Lundberg, M., Yan, J. J., Weng, T. C., Sokaras, D., Alonso-Mori, R., Casa, D., Upton, M. H., Hedman, B., Hodgson, K. O., and Solomon, E. I. (2014) Resonant inelastic X-ray scattering on ferrous and ferric bis-imidazole porphyrin and cytochrome c: nature and role of the axial methionine-Fe bond, *J Am Chem Soc 136*, 18087-18099.
[70] Mara, M. W., Hadt, R. G., Reinhard, M. E., Kroll, T., Lim, H., Hartsock, R. W., Alonso-Mori, R., Chollet, M., Glownia, J. M., Nelson, S., Sokaras, D., Kunnus, K., Hodgson, K. O., Hedman, B., Bergmann, U., Gaffney, K. J., and Solomon, E. I. (2017) Metalloprotein entatic control of ligand-metal bonds quantified by ultrafast x-ray spectroscopy, *Science 356*, 1276-1280.
[71] Vallee, B. L., and Williams, R. J. (1968) Metalloenzymes: the entatic nature of their active sites, *Proc Natl Acad Sci U S A 59*, 498-505.
[72] McClelland, L. J., Mou, T. C., Jeakins-Cooley, M. E., Sprang, S. R., and Bowler, B. E. (2014) Structure of a mitochondrial cytochrome c conformer competent for peroxidase activity, *Proc Natl Acad Sci U S A 111*, 6648-6653.
[73] Robinson, M. N., Boswell, A. P., Huang, Z. X., Eley, C. G., and Moore, G. R. (1983) The conformation of eukaryotic cytochrome c around residues 39, 57, 59 and 74, *Biochem J 213*, 687-700.

[74] Schejter, A., Koshy, T. I., Luntz, T. L., Sanishvili, R., Vig, I., and Margoliash, E. (1994) Effects of mutating Asn-52 to isoleucine on the haem-linked properties of cytochrome c, *Biochem J 302 (Pt 1)*, 95-101.
[75] Maity, H., Rumbley, J. N., and Englander, S. W. (2006) Functional role of a protein foldon--an Ω-loop foldon controls the alkaline transition in ferricytochrome c, *Proteins 63*, 349-355.
[76] Assfalg, M., Bertini, I., Dolfi, A., Turano, P., Mauk, A. G., Rosell, F. I., and Gray, H. B. (2003) Structural model for an alkaline form of ferricytochrome C, *J Am Chem Soc 125*, 2913-2922.
[77] Huttemann, M., Lee, I., Pecinova, A., Pecina, P., Przyklenk, K., and Doan, J. W. (2008) Regulation of oxidative phosphorylation, the mitochondrial membrane potential, and their role in human disease, *J Bioenerg Biomembr 40*, 445-456.
[78] Huttemann, M., Lee, I., Grossman, L. I., Doan, J. W., and Sanderson, T. H. (2012) Phosphorylation of mammalian cytochrome c and cytochrome c oxidase in the regulation of cell destiny: respiration, apoptosis, and human disease, *Advs Expt Med Biol 748*, 237-264.
[79] Lee, I., Salomon, A. R., Yu, K., Doan, J. W., Grossman, L. I., and Huttemann, M. (2006) New prospects for an old enzyme: mammalian cytochrome c is tyrosine-phosphorylated in vivo, *Biochemistry 45*, 9121-9128.
[80] Yu, H., Lee, I., Salomon, A. R., Yu, K., and Huttemann, M. (2008) Mammalian liver cytochrome c is tyrosine-48 phosphorylated in vivo, inhibiting mitochondrial respiration, *Biochim Biophys Acta 1777*, 1066-1071.
[81] Mahapatra, G., Varughese, A., Ji, Q., Lee, I., Liu, J., Vaishnav, A., Sinkler, C., Kapralov, A. A., Moraes, C. T., Sanderson, T. H., Stemmler, T. L., Grossman, L. I., Kagan, V. E., Brunzelle, J. S., Salomon, A. R., Edwards, B. F., and Huttemann, M. (2017) Phosphorylation of Cytochrome c Threonine 28 Regulates Electron Transport Chain Activity in Kidney: IMPLICATIONS FOR AMP KINASE, *J Biol Chem 292*, 64-79.
[82] Pecina, P., Borisenko, G. G., Belikova, N. A., Tyurina, Y. Y., Pecinova, A., Lee, I., Samhan-Arias, A. K., Przyklenk, K., Kagan, V. E., and Huttemann, M. (2010) Phosphomimetic substitution of cytochrome C tyrosine 48 decreases respiration and binding to cardiolipin and abolishes ability to trigger downstream caspase activation, *Biochemistry 49*, 6705-6714.
[83] Garcia-Heredia, J. M., Diaz-Moreno, I., Diaz-Quintana, A., Orzaez, M., Navarro, J. A., Hervas, M., and De la Rosa, M. A. (2012) Specific nitration of tyrosines 46 and 48 makes cytochrome c assemble a non-functional apoptosome, *FEBS Lett 586*, 154-158.
[84] Moreno-Beltran, B., Guerra-Castellano, A., Diaz-Quintana, A., Del Conte, R., Garcia-Maurino, S. M., Diaz-Moreno, S., Gonzalez-Arzola, K., Santos-Ocana, C., Velazquez-Campoy, A., De la Rosa, M. A., Turano, P., and Diaz-Moreno, I. (2017) Structural basis of mitochondrial dysfunction in response to cytochrome c phosphorylation at tyrosine 48, *Proc Natl Acad Sci U S A 114*, 3041-3050.
[85] Moore, G. R., and Pettigrew, G. W. (1990) Cytochrome c: Evolutionary, Structural and Physicochemical Aspects, *Springer-Verlag, London.*

For Table of Contents Use Only

Heightened dynamics of the oxidized Y48H variant of human cytochrome *c* increases its peroxidatic activity

Oliver M. Deacon, Andreas Ioannis Karsisiotis, Tadeo Moreno-Chicano, Michael A. Hough, Colin Macdonald, Tharin M.A. Blumenschein, Michael T. Wilson, Geoffrey R. Moore, Jonathan A.R. Worrall